A Conservative Numerical Model for Vortex Merger

By BALU T. NADIGA[1], AND STEVE SHKOLLER[2] †

[1]Earth and Environmental Sciences, MS-C305, Los Alamos NM 87545 USA
email:balu@lanl.gov

[2]Department of Mathematics, University of California, Davis CA 95616 USA
email:shkoller@math.ucdavis.edu

(Received ?? and in revised form ??)

This paper is devoted to a derivation and numerical implementation of a conservative system of PDEs written in vorticity form as

$$\dot{\omega}^\epsilon + (1-\epsilon\triangle)^{-1}\{\psi^\epsilon, (1-\epsilon\triangle)\omega^\epsilon\} = 0,$$

where the stream function $\psi^\epsilon = (-\triangle)^{-1}\omega^\epsilon$. When $\epsilon = \alpha^2$, where α is a small length scale, this system is the averaged Euler or Euler-α equation, which models the flow of incompressible fluids at length scales larger than α. On the other hand, when $\epsilon = \tilde{\alpha}_1$, a fixed material constant of the fluid, this PDE is the equation of motion for non-newtonian second-grade fluids.

Remarkably, this PDE is the geodesic of a right invariant H^1 metric on the group of volume preserving diffeomorphisms of the fluid container, and formally converges to the Euler equations as $\epsilon \to 0$, thus providing a dispersive (as opposed to viscous) regularization of the Euler equations and a natural *conservative* numerical algorithm.

We present a series of two dimensional, numerical computations comparing the Euler, Navier-Stokes, and Euler-α equations, and show that the conservative Euler-α evolution is able to model the phenomenon of vortex merger. In particular, we show that although this new system retains an infinite number of Casimir functions, the α-enstrophy sharply decays during the vortex merger process and evolves toward a quasi-steady state, qualitatively mimicking the enstrophy characteristics of the dissipative Navier-Stokes system. This suggests that viscous *selective-decay* arguments may not be necessary for describing the emergence of coherent structures in two-dimensional flows.

1. Introduction

The Euler equations of ideal incompressible hydrodynamics on a two dimensional Riemannian manifold M may be expressed in vorticity form as

$$\begin{gathered}\dot{\omega}(t) + \nabla_{u(t)}\omega(t) = 0,\\ \text{div } u(t) = 0, \quad \omega(0) = \omega_0,\end{gathered} \tag{1.1}$$

where ∇ denotes the covariant derivative, ω is the vorticity function, and u is the spatial velocity field with flow $\eta(t)$ satisfying

$$\dot{\eta}(t) = u(\eta(t)).$$

† Present address: Center for Nonliear Studies, Los Alamos National Laboratory, MS-B258, Los Alamos NM 87545

Herein, we shall use the overdot for the partial time derivative. Equivalently, (1.1) may be expressed as the conservation law

$$\frac{d}{dt}\omega(t,\eta(t)) = 0, \tag{1.2}$$

which expresses the condition that the flow is isovorticed; that is, vorticity is constant along the fluid particle trajectories. Isovorticity has the geometric interpretation as a condition on phase points which constrains them to belong to the same coadjoint orbit; these are subsets of phase space that are left invariant by the flow $\eta(t)$ and along which vorticity remains constant. Having this invariance property, solutions of the Euler equations necessarily prevent vortex merging from occurring; rather, two like-sign vortices (which are sufficiently close together) wind into one another causing long thin filamentation.

Coadjoint orbits are distinguished by the values of the first integrals of the motion which include the vorticity momenta, the first of which corresponds to the enstrophy, $\int_M \omega(x)^2\mu(x)$. Hence, in order to model vortex merger, a mechanism must be added to allow for the necessary break of isovorticity. Traditionally, viscous dissipation has been the most commonly used mechanism, forcing the fluid trajectory to leave the original (initial) coadjoint orbit and move transversally through the invariant sets of the Euler flow, effectively sliding from one coadjoint orbit onto another. Numerical simulations of the 2D Navier-Stokes equations provide evidence of such behavior; namely, an examination of the graph of enstrophy versus time shows significant decay during vortex merging, followed by evolution toward a quasi-steady state (see, e.g., Matthaeus & Montgomery (1980), McWilliams (1984), and Overman & Zabusky (1982)). This behavior is one of the distinguishing features of two dimensional fluid turbulence.

While the addition of viscosity provides a nice numerical model for the merging of vortices, the dissipation can eventually eliminate relevant features of the solution, particularly in longtime simulations. After all, the viscosity in the Navier-Stokes equations is the molecular viscosity of the fluid, and this number is typically orders of magnitude smaller than the number required for numerical simulations. This is true, for example, in numerical simulations of Jupiter's red spot as well as in simulations of the ocean, and thus motivates the development of numerical models that do not require dissipative mechanisms, and which can simultaneously capture the qualitative features of the solution.

At least one such conservative model is provided by the **averaged Euler (Euler-α) equation** or equivalently, the equation of motion for **second-grade non-newtonian fluids**, a system of PDEs depending on a parameter ϵ and given by

$$\begin{gathered}\dot{\omega}^\epsilon + (1-\epsilon\triangle)^{-1}\nabla_{u^\epsilon}(1-\epsilon\triangle)\omega^\epsilon = 0\\ \operatorname{div}\, u^\epsilon(t) = 0, \quad \omega^\epsilon(0) = \omega_0^\epsilon,\end{gathered} \tag{1.3}$$

where $\triangle$ is the Laplacian on vector fields. The two interpretation for this model are as follows:

(A) If $\alpha > 0$ is a small length scale and we set $\epsilon = \alpha^2$, then solutions of (1.3) may be viewed as the ensemble-averaged component of the flow of the Euler equation (1.1) (see Marsden, Ratiu & Shkoller (1999b)). In this case, a new vorticity field ω^α is advected by its filtered (or averaged) spatial velocity field u^α. As $\alpha \to 0$, the Euler equations (1.1) are recovered, so (1.3) may be viewed as a dispersive, rather than dissipative, regularization of the Euler equations, and thus naturally provides a *conservative* numerical algorithm that models vortex merger without the addition of *artificial* viscosity.

(B) If we set ϵ to be a material constant $\tilde{\alpha}_1$ denoting the elastic response of the fluid, then (1.3) is exactly the model for inviscid second-grade non-newtonian fluids (see

Rivlin & Ericksen (1955), Noll & Truesdell (1965), and Dunn & Fosdick (1974)). This evolution equation is obtained from the unique Rivlin-Ericksen constitutive law that satisfies material frame indifference and observer objectivity.

As we shall describe, the conservative PDE (1.3) has an infinite number of conservation laws (Casimirs), but the kinetic energy of the α-vorticity field, $\int_M \omega^\alpha(t,x)^2 dx$, is not constrained to be constant; in sharp constrast, when plotted as a function of time, this quantitiy exhibits the correct enstrophy decay that is characteristic of the vorticity mixing process.

In the context of interpretation B, these equations have been known for over thirty-five years (see Noll & Truesdell (1965) and references therein). Interpretation A, on the other hand, is relatively new and first appeared in Holm, Marsden & Ratiu (1998a) and Holm, Marsden & Ratiu (1998b). The geometry and functional-analytic properties of this conservative system was first considered by Shkoller (1998) on boundaryless n dimensional Riemannian manifolds, and by Marsden, Ratiu & Shkoller (1999a) on manifolds with boundary. The mathematical analysis of the corresponding viscous equations can be found in Cioranescu & Ouazar (1984), Cioranescu & Girault (1997), Galdi, Grobbelaarvandalsen, & Sauer (1993), and Foias, Holm & Titi (1999).

In this article, we shall focus on interpretation A; in particular, we shall take a numerics point-of-view and show that these equations have the useful property of reducing resolution requirements when studying the dynamics of the Euler equation, and doing so in a conservative framework. We shall discuss in some detail the geometric properties of the Euler-α equations in Section 2.

In Section 3, we shall present a series of results from numerical simulations. We have used a fully dealiased pseudo-spectral spatial discretization together with a fifth-order adaptive embedded Runge-Kutta Cash-Karp temporal discretization to solve the Euler, Navier-Stokes, and Euler-α equations. For the conservative Euler and Euler-α systems, this algorithm preserves the energy and the first integral of motion to machine precision.

We consider the same initial condition for all three models (appropriately filtered for the Euler-α equation) consisting of essentially two smooth large scale vortex patches of positive sign and two of negative sign (together with other smaller vortex patches). We use 170 modes consisting of 85 sines and cosines for all of our numerical simulations. Fixing this resolution, our numerical results, displaying the evolution of the three truncated systems, support our assertions. Namely, we see that the truncated Euler equations are not able to model vortex merger, but rather, that a collection of tiny vortex fragments are formed. On the other hand, the truncated Navier-Stokes system nicely models the merging phenomenon, but requires a large viscosity (to obtain numerical resolution) which causes a 10% decrease in energy during the course of the simulation (92 eddy turnovers); as a consequence, the vorticity field becomes overly smoothed indicating that longtime simulations may remove relevant features of the solution. We then solve the truncated Euler-α equation, and find that with zero dissipation, the dynamics are qualitatively similar to those of the truncated Navier-Stokes system.

To our knowledge, this is the first example of an evolution toward a quasi-steady dipolar state that does not rely on viscous *selective-decay* processes (see, for example, Matthaeus & Montgomery (1980)), and hence supports the inviscid statistical theories for large-scale coherent structure formation in two-dimensional turbulence (see, for example, Kraichnan & Montgomery (1967), Robert & Sommeria (1991), Miller, Weichman, & Cross (1992), and Majda & Holen (1997)).

Finally, in Appendix A we give a brief review of the Euler-Poincaré reduction theorem in the context of geodesic flow on the volume preserving diffeomorphism group and the Arnold framework of ideal incompressible hydrodynamics.

2. Derivation the Euler-α Equations

The derivation we present for the Euler-α equations is based on two ideas: 1) filtering of small spatial scales, and 2) symmetry reduction. Appendix A contains a discussion of the volume-preserving diffeomorphism group as the configuration space of ideal incompressible hydrodynamics, as well as a discussion of Euler-Poincaré reduction.

We refer the reader to Rivlin & Ericksen (1955), Noll & Truesdell (1965), and Dunn & Fosdick (1974) for the original derivation based on continuum mechanics and the Rivlin-Ericksen tensors. We also refer the reader to Holm, Marsden & Ratiu (1998b) for an alternative derivation of this equation on the full Euclidean space $\mathbb{R}^n$, and to Marsden, Ratiu & Shkoller (1999a) for an instrinsic derivation using the structure of the volume preserving diffeomorphism group.

2.1. *Diffeomorphism Groups*

We consider the motion of an ideal incompressible fluid filling a container M which we assume is a Riemannian manifold with metric g and volume form μ. The **configuration space** for ideal incompressible hydrodynamics is the group $\mathcal{D}_\mu(M)$ consisting of all diffeomorphisms of M preserving the volume form μ. The group operation is composition from the right; if η_1 and η_2 are in $\mathcal{D}_\mu(M)$, then their composition, denoted by $\eta_1 \circ \eta_2$ is in $\mathcal{D}_\mu(M)$. If the fluid container has a boundary ∂M, then elements of $\mathcal{D}_\mu(M)$ must additionally leave the boundary ∂M invariant. For the purpose of this exposition it will suffice to suppose all objects are as smooth necessary. We refer the interested reader to Ebin & Marsden (1970) for a rigorous treatment of the functional analytic properties of Hilbert diffeomorphism groups.

2.2. *Lie Algebra*

The **Lie algebra** of the group $\mathcal{D}_\mu(M)$ is, by definition, the tangent space to $\mathcal{D}_\mu(M)$ at the identity element $e \in \mathcal{D}_\mu(M)$ (the identity element e is defined by $e(x) = x$ for all x in M). We shall denote the Lie algebra by $\mathcal{V}_\mu(M)$; this is the vector space consisting of the smooth divergence-free vector fields on M which are tangential to the boundary ∂M whenever the fluid container has a nonempty boundary. The **Lie bracket** of two element u, v in $\mathcal{V}_\mu(M)$ is given by

$$[u, v] = \nabla_v u - \nabla_u v, \tag{2.1}$$

where ∇ is the unique metric-compatible covariant derivative on M.

Note that for a rigorous treatment of the diffeomorphism group, one must consider the larger topological group $\mathcal{D}^s_\mu(M)$ consisting of bijective mappings of Hilbert class H^s with H^s inverses. The group $\mathcal{D}^s_\mu(M)$ is not a Lie group, and its tangent space at the identity is not, strictly speaking, a Lie algebra. See Ebin & Marsden (1970) and Shkoller (1998) for further details.

2.3. *Euler-α equations*

Our objective here is to obtain an evolution equation which **filters** the small spatial scales in the fluid motion, but does so in a conservative structure-preserving fashion; consequently, unlike methods which rely on viscous dissipation to smooth-out or filter the small-scale (or subgrid) fluid motion, our resulting conservative evolution law allows for the accurate *longtime* numerical integration without dissipating the key features of the solution.

As we shall show, the idea of filtering small or (numerically) unresolvable spatial scales happens to coincide with regularization of the geodesic flow on the group of volume preserving diffeomorphisms $\mathcal{D}_\mu(M)$. We begin by defining the large scale motion of the fluid as motion corresponding to all spatial scales larger than some $\alpha > 0$. Thus, we shall obtain a one-parameter family of evolution laws depending on the length scale α. For each $\alpha > 0$, we define u^α to be the **filtered spatial velocity field** whose motion is representative of the *large spatial scales* of the fluid. When $\alpha = 0$, no filtering occurs, and so the Euler velocity field $u := u^0$ may be viewed as a regular limit of u^α as $\alpha \to 0$.

To begin, we filter the small scales in the initial velocity field u_0 in the Euler system (A 3). Letting $\triangle$ denote the Laplacian on vector fields†, we define

$$u^\alpha(0) = (1 - \alpha^2 \triangle)^{-\frac{1}{2}} u_0. \tag{2.2}$$

For example, when considering flow with periodic boundary conditions, the Fourier representation of this relation is given by

$$u_k^\alpha(0) = \frac{u_k(0)}{(1 + \alpha^2 k^2)^{\frac{1}{2}}}; \tag{2.3}$$

thus, as $|k|$ becomes larger that $1/\alpha$, the terms in the Fourier series corresponding to the kth wave number become smaller and smaller, until their contribution is negligible.

In Appendix A, we remind the reader that solutions of the Euler equations are geodesics of the kinetic energy or L^2 metric on $\mathcal{V}_\mu(M)$. For the purposes of deriving the Euler-α equations, let us now define a different metric on the Lie algebra $\mathcal{V}_\mu(M)$. For any u, v in $\mathcal{V}_\mu(M)$, the H^1_α **metric** is given by (we are using g to denote the metric on M)

$$\langle u, v\rangle_{H^1_\alpha} = \int_M \left[g_x(u(x), v(x)) + \alpha^2 g_x(\nabla u(x), \nabla v(x))\right] \mu(x). \tag{2.4}$$

Integrating by parts, we obtain that

$$\begin{aligned} \langle u, v\rangle_{H^1_\alpha} &= \int_M g_x\left((1 - \alpha^2\triangle)u(x), v(x)\right)\mu(x) \\ &= \int_M g_x\left((1 - \alpha^2\triangle)^{\frac{1}{2}}u(x), (1 - \alpha^2\triangle)^{\frac{1}{2}}v(x)\right)\mu(x), \end{aligned} \tag{2.5}$$

for any pair of vectors u and v in the Lie algebra $\mathcal{V}_\mu(M)$. We have used the fact that either ∂M is empty or u and v satisfy boundary conditions that cause the boundary integral term to vanish (see Marsden, Ratiu & Shkoller (1999a) for the appropriate boundary conditions).

The evolution equations for u^α will arise as the Euler-Poincaré equations of a new **filtered action** function s^α, defined on curves in $\mathcal{V}_\mu(M)$. Our criteria for defining the filtered action function s^α is simply that $s^\alpha(u^\alpha) = s(u)$ on any time interval. From (2.2), $(1 - \alpha^2\triangle)^{\frac{1}{2}} u^\alpha(0) = u(0)$, so we define the filtered action by

$$s^\alpha(u^\alpha) = \int \langle u^\alpha(t), u^\alpha(t)\rangle_{H^1_\alpha} dt. \tag{2.6}$$

Thus, we see that the filtered action is given by a modified H^1_α energy, i.e. $l^\alpha(u^\alpha) = (1/2)\langle u^\alpha, u^\alpha\rangle_{H^1_\alpha}$. (See Appendix A for an explanation of the notation used here.)

One may picture our filtering procedure as replacing a fluid particle with a **fluid blob**, so that in addition to the usual kinetic energy of the particle, now viewed as the center of the blob, additional energy is added by the small fluctuations of the fluid blob. This follows from (2.4).

† If M is an open subset of Euclidean space $\mathbb{R}^n$, then $\triangle$ denotes the component-wise Laplacian which, in local coordinates, acts on each component of the vector field by $-\frac{\partial^2}{\partial x^i \partial x^i}$. In the case that M is a Riemannian manifold, then $\triangle$ denotes the Laplace de-Rham operator given by $\triangle = d\delta + \delta d$, where d is the exterior derivative, and δ is its formal adjoint.

Just as with the L^2 metric, we can right translate the H^1_α metric over the entire volume preserving diffeomorphism group, to obtain a right invariant system on $\mathcal{D}_\mu(M)$ (see (2.6) in Shkoller (1998)). Critical points of the unreduced action function S^α formed from this right invariant metric on $\mathcal{D}_\mu(M)$ coincide with geodesics of the H^1_α metric, in perfect analogy with the way that the usual Euler flow coincides with the right invariant L^2 geodesic motion. We shall use the Euler-Poincaré theorem to find the system of PDEs that such a **regularized geodesic** must satisfy, i.e. we compute the critical points of the reduced filtered action s^α.

With respect to the H^1_α metric, the functional derivative $\frac{\delta l^\alpha}{\delta u^\alpha}$ of the **filtered reduced Lagrangian** l^α is equal to u^α. A computation of $\mathrm{ad}^*_{u^\alpha} u^\alpha$ with respect to the metric (2.4) yields (see Shkoller (1998) and Marsden, Ratiu & Shkoller (1999a))

$$\mathrm{ad}^*_{u^\alpha} u^\alpha = (1-\alpha^2\triangle)^{-1}\left[\nabla_{u^\alpha}(1-\alpha^2\triangle)u^\alpha - \alpha^2[\nabla u^\alpha]^T \cdot \triangle u^\alpha + \mathrm{grad}\, p^\alpha\right]. \tag{2.7}$$

Hence, we obtain the **Euler-α equation** or equivalently the **equations of second-grade non-newtonian fluids** as

$$\begin{gathered} \dot v^\alpha + \nabla_{u^\alpha} v^\alpha - \alpha^2[\nabla u^\alpha]^T \cdot \triangle u^\alpha = -\mathrm{grad}\, p^\alpha, \\ v^\alpha = (1-\alpha^2\triangle)u^\alpha, \quad \mathrm{div}\; u^\alpha = 0, \quad u^\alpha(0) = u^\alpha_0 = (1-\alpha^2\triangle)^{-\frac{1}{2}} u_0, \end{gathered} \tag{2.8}$$

where the pressure function p^α is completely determined by u^α through the Hodge decomposition. This form of the equation is precisely the form in which the second-grade fluids model is typically expressed.

By construction, solutions u^α of the Euler-α equations are conserved in the H^1_α norm, as opposed to the L^2 conservation law for solutions of the usual Euler solution u. For two dimensional flows there are an infinite number of conservation laws, which we shall describe next.

3. The Vorticity Equations

3.1. *The α-vorticity formulation*

We begin by noting that their is a dual representation for the Euler equations when the fields are thought of as 1-forms or covector fields† instead of vector fields (see Arnold & Khesin (1998)); namely if $U = u^\flat$ is the 1-form field associated to the vector field u, then the Euler equations can be expressed as

$$\dot U + \mathcal{L}_u U = -dp, \tag{3.1}$$

where $\mathcal{L}$ denotes the Lie derivative of the 1-form field U in the direction u. Applying the exterior derivative d to equation (3.1), and noting that d commutes with $\mathcal{L}$, one obtains the standard Euler vorticity equations

$$\dot\omega + \mathcal{L}_u \omega = 0, \tag{3.2}$$

where the vorticity 2-form $\omega = dU$. In the case that the fluid container M is two dimensional, we may identify the two form ω with a function on M using the area form μ, in which case the Lie derivative is just the ordinary derivative of functions.

In the stream function formulation, the velocity field u equals $rot(\psi)$ for a stream function ψ so that in local coordinates, the components of u are given by

$$(u^1, u^2) = \left(-\frac{\partial\psi}{\partial x^2}, \frac{\partial\psi}{\partial x^1}\right),$$

† It is standard to use the symbols for the musical maps, $\flat$ and $\sharp$, to denote the mappings from vector fields to 1-forms and from 1-forms to vector fields, respectively.

and the vorticity equations in two dimensions can be written in the familiar Lie-Poisson form

$$\dot{\omega} = -\{\psi, \omega\}, \tag{3.3}$$

where the action of the Poisson bracket is defined by

$$\{\psi, \omega\} = \frac{\partial \psi}{\partial x^2}\frac{\partial \omega}{\partial x^1} - \frac{\partial \psi}{\partial x^1}\frac{\partial \omega}{\partial x^2}.$$

Recall that this two dimensional system has an infinite number of Casimir functions given by

$$\int_M F(\omega)(x)\mu(x),$$

where F is any smooth function.

One may express the Euler-α equations in this dual representation as well. Defining the 1-form field $V^\alpha = (v^\alpha)^\flat$, where $v^\alpha = (1-\alpha^2\triangle)u^\alpha$, equation (2.8) may be written as

$$\dot{V}^\alpha + \mathcal{L}_{u^\alpha} V^\alpha = -dp^\alpha. \tag{3.4}$$

Letting $U^\alpha = (u^\alpha)^\flat$, one may express the α-vorticity equations in two ways. Letting

$$\omega^\alpha = dU^\alpha \text{ and } q^\alpha = dV^\alpha,$$

and applying the exterior derivative d to (3.4), we obtain the **α-vorticity equations** as

$$\dot{\omega}^\alpha + (1-\alpha^2\triangle)^{-1}\mathcal{L}_{u^\alpha}(1-\alpha^2\triangle)\omega^\alpha = 0, \tag{3.5}$$

or

$$\dot{q}^\alpha + \mathcal{L}_{u^\alpha} q^\alpha = 0. \tag{3.6}$$

Again for two dimensional flow, we may identify the 2-forms ω^α and q^α with functions, and express the α-vorticity equations in the Lie-Poisson form

$$\dot{q}^\alpha = -\{\psi^\alpha, q^\alpha\}, \tag{3.7}$$

where ψ^α is the stream function given by $u^\alpha = rot(\psi^\alpha)$ or equivalently by $-\triangle\psi^\alpha = \omega^\alpha$ or by $-(1-\alpha^2\triangle)\triangle\psi^\alpha = q^\alpha$. The α-vorticity equations again (3.7) possesses an infinite number of Casimirs given by

$$\int_M F(q^\alpha)(x)\mu(x),$$

for any smooth function F. The **α-enstrophy** is simply the energy of q^α given by $\langle q^\alpha, q^\alpha\rangle_{L^2}$.

Thus, while solutions of the Euler flow conserve the L^2 norm of the spatial velocity $\langle u, u\rangle_{L^2}$ and the enstrophy $\langle \omega, \omega\rangle_{L^2}$, the Euler-$\alpha$ flow conserves the H^1_α norm of the spatial velocity $\langle u^\alpha, u^\alpha\rangle_{H^1_\alpha}$ and the H^2_α norm of the corresponding vorticity field ω^α given by

$$\langle \omega^\alpha, \omega^\alpha\rangle_{H^2_\alpha} = \int_M [(1-\alpha^2\triangle)\omega^\alpha(x)]^2\mu(x) = \int_M q^\alpha(x)^2\mu(x).$$

For two dimensional periodic flow, integration-by-parts shows that

$$\|u^\alpha(t)\|^2_{H^1_\alpha} = \|u^\alpha(t)\|^2_{L^2} + \alpha^2\|\omega^\alpha(t)\|^2_{L^2} = C^\alpha, \tag{3.8}$$

for some constant C^α depending on the parameter α. By comparison, solutions of the Euler equations satisfy

$$\|u(t)\|^2_{L^2} + \alpha^2\|\omega(t)\|^2_{L^2} = C, \tag{3.9}$$

as well; in this case, however, both kinetic energy and enstrophy are independently conserved (over constraining the system), while the Euler-α system may evolve towards states of minimum enstrophy.

4. Numerical Simulations

In this section, we present results of numerical simulations which show that the conservative Euler-α equations (with small α) are able to capture the vortex merger phenomenon without the addition of viscous dissipation. These simulations are based on the vorticity formulation (3.7) of the Euler-α equation, and the vorticity form of Navier-Stokes given by

$$\dot{\omega} + \{\psi, \omega\} = \nu \triangle \omega, \tag{4.1}$$

where $\nu > 0$ is the viscosity.

We pose the following question in the context of our numerical comparison: How well can one simulate the *longtime* evolution of a given set of initial conditions given an a priori fixed amount of computational resources. For simplicity, we consider a doubly-periodic domain of length 2π on a side, and the initial condition

$$w_0 = (\sin x + \sin 2x) * (\sin y + \sin 2y) \tag{4.2}$$

which is displayed in Figure B.1.

All the simulations presented in this article use a fully dealiased pseudospectral Fourier (Canuto (1988)) spatial discretization (and thus equivalent to Fourier-Galerkin). The dealiasing is achieved using the two-thirds rule (also called the three-halves rule) wherein only two-thirds of the Fourier modes are used and the highest wavenumber-third of the modes are zero-padded. (This is equivalent to computing the nonlinear terms in physical space at three-halves the number of points as the number of Fourier modes used.) With such a discretization, the kinetic energy which we shall denote by K, given by

$$K(\psi) = \int_M |\nabla \psi(x)|^2 dx = \|u\|^2_{L^2}, \tag{4.3}$$

and the enstrophy which we shall denote by Z, given by

$$Z(\omega) = \int_M \omega(x)^2 dx = \|\omega\|^2_{L^2}, \tag{4.4}$$

are identically conserved by the spatial discretization of the Euler equations (3.3). Letting

$$F_\alpha \equiv (1 - \alpha^2 \triangle)^{\frac{1}{2}},$$

we may express the two corresponding quadratic conserved quantities for the Euler-α equations by

$$K(F_\alpha \psi^\alpha) = \int_M |(1 - \alpha^2 \triangle) \nabla \psi^\alpha(x)|^2 dx = \|u^\alpha\|^2_{H^1_\alpha}, \tag{4.5}$$

and

$$Z\left(F_\alpha^2 \omega^\alpha\right) = Z(q^\alpha) = \int_M q^\alpha(x)^2 dx = \|\omega^\alpha\|^2_{H^2_\alpha}. \tag{4.6}$$

We remark that we repeated some of the computations using the Arakawa second-order finite difference spatial discretization; this scheme also conserves the energy and enstrophy, and uses the Arakawa Jacobian, $\mathrm{J}[\psi,\omega]$, for $\{\psi,\omega\}$, and where $\mathrm{J}[\psi,\omega]$ is given by

$$\mathrm{J}[\psi,\omega] = \frac{1}{3}\left(\psi_y\omega_x - \psi_x\omega_y + (\psi_y\omega)_x - (\psi_x\omega)_y + (\psi\omega_x)_y - (\psi\omega_y)_x\right), \tag{4.7}$$

(see Arakawa (1966)). In the above equation, each of the partial derivative is replaced by its central difference quotient. The numerical results this scheme produced were qualitatively identical to the spectral method.

As for the temporal discretization, we use a (nominally) fifth-order adaptive timestep embedded Runge-Kutta Cash-Karp algorithm (see Press et al. (1992)). This scheme is advantageous over the more traditional leapfrog timestepping as it does not have a spurious computational mode and it allows for variable timestepping to be implemented in a straightforward manner. One step of this method uses six functional evaluations at appropriate points which are combined in two different ways to produce a fourth-order and a fifth-order increment, thereby allowing an estimate of the fifth-order error. This method of adaptive timestepping is approximately twice as efficient as Runge-Kutta methods based on timestep doubling. By requiring

$$\frac{\max|E_5(\omega_k,\omega_{k+1})|}{\max|\omega_k|} < 10^{-7},$$

energy error was (on average) less than one hundredth of a percent (0.01%) and enstrophy error was less than one tenth of one percent (0.10%) during the course of the inviscid simulations that we performed.

4.1. *2D Euler Equations*

Figure B.2 shows the vorticity field for the truncated Euler equations at 23, 46, 69, and 92 large eddy turnover times, where a large eddy turnover time is defined as

$$\tau = \frac{2\pi k_i^{-1}}{u'}.$$

Here, k_i represents the integral scale of the initial condition, found as a ratio of the conserved enstrophy to the conserved energy:

$$k_i = \left(\sum_{k=k_{min}}^{k=k_{max}} k^2 E(k)\right)^{\frac{1}{2}} \left(\sum_{k=k_{min}}^{k=k_{max}} E(k)\right)^{-\frac{1}{2}}, \tag{4.8}$$

and the mean fluctuation velocity u' is calculated as

$$u' = \left(2\sum_{k=k_{min}}^{k=k_{max}} E(k)\right)^{1/2}.$$

Henceforth, we shall use **large eddy turnovers** as our standard unit of time. As mentioned earlier, the energy and enstrophy are both very well conserved in this run. As can be seen, a single dipole does not form; rather, a disconnected collection of high- and low-valued vorticity *fragments* is formed. Figure B.3 shows the energy spectra at the same four times. The increase in energy (with time) at the lowest wavenumber shows the upscale cascade of energy and at the same time, the increase in enstrophy $k^2E(k)$ (not shown) at the high wavenumbers indicates the downscale cascade of enstrophy—a characteristic feature of two-dimensional turbulence. It is clearly the downscale cascade of enstrophy which leads very quickly to the computation being under-resolved (indicated by the elevated levels of the energy spectra at the highest resolved wavenumbers). We note however, that the changes in the spectra are quite small between the times 69 and 92 suggesting an equilibration between the finite number of modes in this truncated system. This equilibrium is necessitated by a simultaneous conservation of energy and enstrophy and leads to a *one-dimensional* energy spectrum for the truncated Euler system of the form

$$E(k) \sim \frac{k}{a+bk^2},$$

where a and b are constants depending on the initial conditions and the pair (k_{min}, k_{max}) (see, for example, Kraichnan (1967), Fox & Orszag (1973), and Basdevant & Sadourny (1975)). This implies equipartition of energy for $k \ll k_i$ ($E(k) \sim k$) and equipartition of enstrophy for $k \gg k_i$ ($E(k) \sim k^{-1}$), where k_i is the integral scale associated with the initial condition as in 4.8.

For the given initial condition (4.2), $k_i = 1.98$ so that we are mostly in the enstrophy equipartition region and the k^{-1} slope is clearly verified. This slow fall-off at high k ($E(k) \sim k^{-1}$) accounts for the poor resolution of the numerical simulation beyond a certain small initial time (less than 23 large eddy turnover times).

4.2. *2D Navier-Stokes*

We presently discuss a set of Navier-Stokes simulations in which the viscosity is progressively increased until the flow is marginally resolved. Figure B.4 shows the energy spectrum at time 92 for the four values of viscosity 10^{-7}, 10^{-6}, 10^{-5}, and 5×10^{-5}. The lack of resolution for the small viscosities and the marginal resolution at $\nu = 5 \times 10^{-5}$ is clear from these spectra. More interesting, however, are Figs. B.5 and B.6 which show respectively the time evolution of the enstrophy and the energy for these four viscous runs. In these figures, a significant decrease in enstrophy occurs between times 46 and 69 for the cases with viscosities 10^{-5} and 5×10^{-5}, while energy has a comparatively mild decay. Figure B.7 shows the instantaneous vorticity field for $\nu = 5 \times 10^{-5}$, again at the four times of 23, 46, 69, and 92 eddy turnovers. An examination of this figure reveals that the large decrease in enstrophy is closely related to the merger of the two pairs of like-signed vortices (seen before merger at time 46 and after merger at time 69). Thus, while the Navier-Stokes simulations very nicely capture the vortex merger, approximately 10% of the kinetic energy is lost in the process.

4.3. *2D Euler-α*

Given a domain size of 2π and a maximum wavenumber, k_{max}, of 85, the smallest resolved length in our simulations is about 0.074. We, therefore, consider simulations of the Euler-α equations using three different values of α: $\alpha = 0.1, 0.2$, and 0.4, corresponding to wave numbers k_α ranging from about 63 to about 16. Our motivation is a reduction in the energy content at wavenumbers k, where $k_\alpha < k \leq 85$, to values much lower than in the corresponding Euler ($\alpha = 0$) simulation.

Figure B.8 shows the instantaneous spectra at 92 eddy turnover times for the four cases $\alpha = 0.0$, 0.1, 0.2, 0.4. Since the conserved energy is

$$\sum_{k=k_{min}}^{k=k_{max}} (1+\alpha^2 k^2) k^2 |\hat{\psi_k^\alpha}|^2,$$

as opposed to

$$\sum_{k=k_{min}}^{k=k_{max}} k^2 |\hat{\psi_k}|^2$$

for the Euler case, the one-dimensional energy spectrum, $E(k)$ is actually defined as

$$E(k) = (1+\alpha^2k^2)k^2|\hat{\psi^\alpha}_k|^2$$

so that as before

$$\sum_{k=k_{min}}^{k=k_{max}} E(k)$$

is conserved. Clearly, the most significant differences occur at the large wavenumbers with the energy at high wavenumbers getting smaller with increasing α. Further, the asymptotic slope of the spectra for nonzero α is different from the k^{-1} slope discussed earlier.

In fact, a similar calculation of the one-dimensional energy spectrum assuming conservation of only the kinetic energy $K(F_\alpha\psi^\alpha)$ and the enstrophy $Z(q^\alpha)$ (the two quantities which are conserved by the discrete numerical computation) yields the relation

$$E(k) \sim \frac{k}{a' + b'(1+\alpha^2k^2)k^2},$$

where as before a' and b' are constants depending on the initial conditions and the pair (k_{min}, k_{max}) (see Nadiga & Shkoller (1999)). The asymptotic behavior of the large scales, $k \ll k_i$ is given by an equipartition of the (conserved) kinetic energy, now $K(F_\alpha\psi^\alpha)$, which implies

$$E(k) \sim k \quad \text{for} \quad k \ll k_i.$$

In other words, the scaling of the energy spectrum at large scales is unaltered by the modification of the cascade process in the Euler-α equation as compared to the original Euler equation (see Nadiga & Shkoller (1999)). Next, the asymptotic behavior of small scales, $k \gg k_i$, is given by an equipartition of the (conserved) enstrophy, now $Z(q^\alpha)$, and this implies

$$E(k) \sim k^{-3} \quad \text{for} \quad k \gg k_i.$$

Thus the small scale behavior of the Euler-α model is modified in such a way that the energy falls off much more rapidly at small scales (k^{-3}) as compared to the original Euler equation (k^{-1}).

Since $k_i \approx 2$ for the initial condition (4.2), we are in the enstrophy cascade regime and the k^{-3} slope is verified is Fig. B.8. Noting that the small wavenumber spectrum for α=0.4 significantly departs from the Euler case, we may interpret the results in Fig. B.8 as follows: In comparison to the spectra for the Euler equations, for reasonably small values of α, the Euler-α model preserves the form of the spectrum at scales large compared to α while making the spectrum fall-off much faster at scales comparable to and smaller than α.

In Fig. B.11 we plot two different enstrophies—$Z(F_\alpha^2\omega^\alpha)$ and $Z(F_\alpha\omega^\alpha)$—for each of the four cases α = 0.0, 0.1, 0.2, and 0.4. Clearly for α=0, the two enstrophies are identical and as mentioned before, are constant to within a tenth of a percent during the run; furthermore, for the nonzero α cases, $Z(F_\alpha^2\omega^\alpha)$ is essentially conserved up to machine precision, so that five of the eight time-histories are horizontal in Fig. B.11. Moreover, since $\omega^\alpha(0)$ is a smoothed version of $\omega(0)$ (see (2.2) and (2.3)) and the evolution equation (3.5) evolves the smoothed initial condition $\omega^\alpha(0)$, if we are to compare solutions at a later time t, the evolved $\omega^\alpha(t)$ has to be roughened to $F_\alpha\omega^\alpha(t)$ before being compared with $\omega(t)$. It also follows that the enstrophy of $F_\alpha\omega^\alpha(t)$, $Z(F_\alpha\omega^\alpha)$, should be the enstrophy of dynamical interest in the α-model.

Figure B.11 shows a jump in the enstrophy $Z(F_\alpha\omega^\alpha)$ which is qualitatively similar to the jump in enstrophy seen in Fig. B.5 for the two higher viscosity runs, and we conjecture that this decrease in enstrophy in these conservative runs is again a signature of vortex merger. (Note again that the merger seems to occur earlier with increasing α so that the Euler-α model with α=0.1 is more representative of the inviscid Euler dynamics than the case with α=0.4.) Figures B.9 and B.10 show, respectively, the snapshots of ω^α and $F_\alpha \omega^\alpha$ again at 23, 46, 69 and 92 eddy turnover times. These figures indeed show that the merger of the two pairs of large like-signed vortices has already occurred at time 46 and by time 92, only a dipole structure remains. These vorticity contours should be compared with the vorticity contours of the Euler simulation shown in Fig. B.2; it is quite evident that a significant reduction in the small-scale noisy features (endemic to the Euler simulation) occurs, even though the Euler-α simulation is not fully resolved. Differences in the trajectories of the large vortices as well as in the evolution of small scale features, such as the appearance of a pair of small blue vortices at time 46 unique to the Euler-α simulation, are due to the inherent unpredictability of particle trajectories for these flows; only qualitative or statistical comparisons can be made, and these type of comparisons are in good agreement between the Navier-Stokes and Euler-α simulations.

Figure B.12 shows the energy evolution of both $K(F_\alpha \psi^\alpha) = \|u^\alpha\|_{H^1_\alpha}$ and $K(\psi^\alpha) = \|u\|_{L^2}$, for the four cases α=0, 0.1, 0.2, and 0.4. Since $\|u^\alpha\|_{H^1_\alpha}$ is conserved for any α, only the graphs of $\|u^\alpha\|_{L^2}$ for α=0.1, 0.2 and 0.4 are not constant. As for the other graphs, energy error was bounded by .01%. The fact that $\|u^\alpha\|_{H^1_\alpha}$ is conserved, together with (3.8), implies that whenever the α-enstrophy drops, $\|u^\alpha\|^2_{L^2}$ must increase; this increase is evident during the time interval of vortex merger, and indicates a conversion of small-scale fluctuation energy into mean motion.

Finally, the scatter plots of the instantaneous vorticity $F_\alpha \omega^\alpha$ and streamfunction ψ^α (at 92 large-scale eddy turnovers) are shown in Fig. B.13 for the four cases α=0, 0.1, 0.2, and 0.4. (For reasons of economy, the fields have been averaged onto a 64x64 grid before plotting.) We conjecture from these plots (and the time evolution of the scatter) that the Euler-α model evolves toward a state which prefers a certain nonlinear vorticity-streamfunction relationship; this is a study of future work.

5. Concluding Remarks

5.1. *Further discussion of results*

We have considered the evolution of a given initial condition under the Euler, Navier-Stokes, and the Euler-α equations, with an intent to capture the large-scale inviscid dynamics. Though the initial condition comprised of only a small number of Fourier modes, and corresponded physically to a simple configuration of a few vorticity patches of both signs, they were not balanced with respect to any of the evolution equations, and therefore, nonlinear cascade processes soon excited the full range of modes available in the truncated computations.

Thereafter, while the Euler solutions evolved to a highly fragmented state, the Navier-Stokes solutions (with ν sufficiently large for numerical resolution, yet small enough to permit inviscid interactions) demonstrated the phenomenon of enstrophy decay wherein like signed vortices merged to evolve into a quasi-steady dipolar state. During this process, unlike the rather abrupt decrease in enstrophy, energy continued to decay smoothly and slowly. Nevertheless, this decay in energy in the Navier-Stokes solution is inevitable. On the other hand, the Euler-α solutions captured the good aspects of both the Euler and the Navier-Stokes solutions: While conserving the two quadratic invariants of energy $K(F_\alpha \psi^\alpha)$ and enstrophy $Z(F^2_\alpha \omega^\alpha)$ as in the Euler solutions, it was able to model vortex merger and captured the associated decay of (now, the $Z(F_\alpha \omega^\alpha)$) enstrophy, as in the Navier-Stokes solutions.

Statistical equilibration arguments based on the conservation of the two quadratic quantities of energy and enstrophy when applied to the Euler and the Euler-α equations, yield similar scalings for the spectra in the energy equipartition region, but with a much steeper slope (k^{-3}) for the Euler-α equations compared to the k^{-1} slope for the Euler equations in the enstrophy equipartition region. Thus, by altering the nonlinear cascade process, the Euler-α equations preserve the large scale features of the Euler flow, while simultaneously suppressing (unwanted) small-scale activity; therein lies the advantage of these models from a numerical point-of-view. We remark, however, that there is considerable work in progress which aims to exploit this feature, but with additional viscosity, to model different aspects of turbulence (see Chen, Foias, Holm, Olson, Titi, & Wynne (1998) and Chen, Holm, Margolin, & Zhang (1999); for a geophysical application see Nadiga & Margolin (1999)).

5.2. *The regular limit of zero viscosity*

In the study of second-grade non-newtonian fluids, a viscosity term is generally included in the equation of motion (see, for example, Dunn & Fosdick (1974)). Therefore, the viscous analog of the Euler-α equations are the viscous equations of second-grade fluids, and are given by

$$\begin{gathered}(1-\alpha^2\triangle)\dot{u}^\alpha - \nu\triangle u^\alpha + \left[\nabla_{u^\alpha}(1-\alpha^2\triangle)u^\alpha - \alpha^2[\nabla u^\alpha]^T \cdot \triangle u^\alpha\right] = -\text{grad } p^\alpha, \\ \text{div } u^\alpha = 0, \quad u^\alpha(0) = u_0^\alpha. \end{gathered} \tag{5.1}$$

Now it is well known that solutions of the Navier-Stokes equations on manifolds with boundary do not converge to solutions of the Euler equations because of the formation of a boundary layer due to a mismatch in boundary conditions; spatial velocity fields solving the Euler equations only have a vanishing normal component on the boundary, while solutions of the Navier-Stokes equations require all components of the velocity to vanish on the boundary. Recently, Barenblatt & Chorin (1998a) and Barenblatt & Chorin (1998b) showed that certain average properties of the flow possess well-defined limits as the viscosity tends to zero. As we have described in interpretation A of the Introduction, solutions of the Euler-α equations may be interpreted as the (ensemble) averaged component of the Euler flow. Marsden, Ratiu & Shkoller (1999a) have shown that solutions of (5.1) converge to solutions of the Euler-α equations even on manifolds with boundary. This may be attributed to the fact that the inviscid Euler-α equations are well-posed with either of the boundary conditions

$$u = 0$$

or

$$g(u^\alpha, n) = 0, \quad (\nabla_n u^\alpha)^{tan} + S_n(u^\alpha) = 0,$$

where n is the outward normal on the boundary, $(\cdot)^{tan}$ denotes the tangential component and S_n is the second fundamental form of the boundary.

5.3. *Statistical convergence of Euler solutions*

We remark here that ensemble-averaged solutions of the Euler equations have been shown to converge to states of maximum entropy in a statistical sense (see, e.g., Majda & Holen (1997)), wherein the vorticity-streamfunction relationship is nonlinear. Again, noting that the solutions of the Euler-α system can be interpreted as the ensemble-averaged component of the Euler flow, it is quite interesting to see that the Euler-α evolution, with no possibility for viscous *selective-decay*, evolved towards a quasi-steady state with a nonlinear vorticity-streamfunction relationship and a much lower value of the $Z(F_\alpha \omega^\alpha)$ enstrophy. It remains to be seen whether this behavior shall persist for a completely general class of initial data, and this is the subject of ongoing work.

5.4. *Lagrangian Stability*

Since solutions to the Euler and Euler-α equations are geodesics of right invariant metrics on the group of smooth fluid configurations $\mathcal{D}_\mu(M)$, one can study their **Lagrangian stability** by considering the behavior of nearby geodesics. A Lagrangian flow $\eta(t)$ is Lagrangian stable if all geodesics in $\mathcal{D}\mu(M)$ with sufficiently close initial conditions at $t = 0$ remain close for all $t \geq 0$.

The Riemannian curvature of a manifold has a profound impact on the behavior of geodesics on it. For manifolds with positive curvature, nearby geodesics usually oscillate about one another, while on manifolds with negative curvature, geodesics rapidly diverge from one another and in this case, the geodesic motion is unstable.

Arnold (1966) computed the sectional curvature of the L^2 metric on the group of smooth fluid configurations of the flat two torus $\mathcal{D}_\mu(\mathbb{T}^2)$ (two dimensional periodic flow) and found that it was negative in 'most' directions.

Shkoller (1998) has proven that the Riemannian curvature operator of the H^1_α metric is a continuous operator, and Pekarsky & Shkoller (1999) have shown that the sectional curvature of the H^1_α metric is positive in many directions. This suggests that the Euler-α model can stabilize the Lagrangian trajectories of an ideal incompressible fluid.

Acknowledgments

The authors would like to thank Vageli Coutsias, Richard Greatbatch, Darryl Holm, Glenn Iereley, Don Jones, Len Margolin, Jerry Marsden, Robert McLachlan, Sergey Pekarsky, and Tudor Ratiu for extensive discussions on a variety of issues related to this article. We are particularly indebted to Rich Jordan for his numerous remarks concerning early drafts, and for directing us to many of the references in the literature concerning this topic. BTN was supported by the Climate Change Prediction Program of the Department of Energy and SS was partially supported by the DOE and by the NSF-KDI grant ATM-98-73133.

Appendix A. Euler-Poincaré Reduction and the Group of Volume Preserving Diffeomorphisms

A.1. L^2 *Right invariant metric on* $\mathcal{D}_\mu(M)$

The metric g and the volume form μ on M induce a natural metric on $\mathcal{V}_\mu(M)$. For two elements u_e, v_e in $\mathcal{V}_\mu(M)$, we define this metric by

$$\langle u_e, v_e \rangle_{L^2} = \int_M g_x(u_e(x), v_e(x))\mu(x). \tag{A 1}$$

This is the L^2 **metric** on divergence-free vector fields on M. The operation of right translating a divergence-free vector u in $\mathcal{V}_\mu(M)$ to any other tangent space to the group $\mathcal{D}_\mu(M)$ is a smooth operation, which does not change the length of the vector u with respect to the L^2 metric. Recall that the map which right translates a vector u in $\mathcal{V}_\mu(M) := T_e\mathcal{D}_\mu(M)$ to $T_\eta\mathcal{D}_\mu(M)$ for any element η in $\mathcal{D}_\mu(M)$, is the map

$$u \mapsto u \circ \eta.$$

Let us denote $u \circ \eta$ by u_η and $v \circ \eta$ by v_η. Then by the change of variables formula together with the fact that $\det T\eta = 1$, we have that for u_η, v_η in $T_\eta \mathcal{D}_\mu(M)$,

$$\langle u_\eta, v_\eta \rangle_{L^2} = \int_M g_{\eta(x)}(u(\eta(x)), v(\eta(x)))\mu(\eta(x)). \tag{A 2}$$

This defines the L^2 **metric on the entire group** $\mathcal{D}_\mu(M)$, and as we just observed, this metric is right invariant. See Arnold (1966), Ebin & Marsden (1970), Marsden & Ratiu (1999), and Arnold & Khesin (1998) for a detailed account.

A.2. *Ideal hydrodynamics*

Let $\eta(t)$ be a smooth curve in $\mathcal{D}_\mu(M)$; then for each time t, the **material velocity** of the fluid $\dot\eta(t)$ is a tangent vector in the tangent space $T_{\eta(t)}\mathcal{D}_\mu(M)$. For each t, we may right translate $\dot\eta(t)$ to the Lie algebra $\mathcal{V}_\mu(M)$ by $\eta(t)^{-1}$, to obtain the Eulerian or **spatial velocity** field $u(t)$.

Arnold (1966) showed that the Eulerian curve

$$u(t) = \dot\eta(t) \circ \eta(t)^{-1} \text{ in } \mathcal{V}_\mu(M)$$

is a solution of the Euler equations

$$\begin{gathered} \partial_t u(t) + \nabla_{u(t)} u(t) = -\operatorname{grad} p(t) \\ \operatorname{div} u(t) = 0, \quad u(0) = u_0, \end{gathered} \tag{A 3}$$

where $p(t)$ is the pressure function completely determined by $u(t)$, if and only if the curve $\eta(t)$ in $\mathcal{D}_\mu(M)$ is a geodesic of the right invariant L^2 metric (A 2) on $\mathcal{D}_\mu(M)$. Motion of the fluid $\eta(t)$ over the entire group $\mathcal{D}_\mu(M)$ is the Lagrangian picture of fluids, while the equations (A 3) describe the Eulerian picture.

In the Eulerian description, one is only interested in the spatial velocity field $u(t)$, while in the Lagrangian framework, one must simultaneously solve for the material velocity field $\dot\eta(t)$ as well as the fluid configuration $\eta(t)$. The Eulerian description is a **symmetry reduction** of the Lagrangian framework. The symmetry here is the particle relabelling symmetry of hydrodynamics given by the action of $\mathcal{D}_\mu(M)$ on itself (or more precisely, by the lifted action of $\mathcal{D}_\mu(M)$ on $T\mathcal{D}_\mu(M)$). In particular, the right invariance of the L^2 metric (A 2) is simply stating that the length of a divergence-free vector v at η is not altered by simply relabeling the current particle configuration η.

A.3. *Euler-Poincaré Reduction*

The reduction onto the Eulerian representation is an example of the Euler-Poincaré theorem (see, for example, Arnold & Khesin (1998) or Marsden & Ratiu (1999)) which we shall now state in the setting of a general Lie group G. For any element η of the Lie group, we shall denote by TR_η the right translation map on the TG, so that for example, when $G = \mathcal{D}_\mu(M)$, then $TR_{\eta^{-1}}\dot\eta := \dot\eta \circ \eta^{-1}$.

Theorem A.1 (Euler-Poincaré). *Let G be a group with smooth right translation, and let $L : TG \to \mathbb{R}$ be a right invariant Lagrangian. Let $\mathfrak{g}$ denote the Lie algebra of G, and let $l : \mathfrak{g} \to \mathbb{R}$ be the restriction of L to $\mathfrak{g}$. For a curve $\eta(t)$ in G, let $u(t) = TR_{\eta(t)^{-1}}\dot\eta(t)$. Then the following are equivalent:*

a *the curve $\eta(t)$ satisfies the Euler-Lagrange equations on G;*

b *the curve $\eta(t)$ is an extremum of the action function*

$$S(\eta) = \int L(\eta(t), \dot\eta(t))dt,$$

for variations $\delta\eta$ with fixed endpoints;

c *the curve $u(t)$ solves the Euler-Poincaré equations*

$$\frac{d}{dt}\frac{\delta l}{\delta u} = -ad^*_u \frac{\delta l}{\delta u},$$

where the coadjoint action ad^*_u is defined by

$$\langle ad^*_u v, w\rangle = \langle v, -[u,w]\rangle,$$

for u, v, w in $\mathfrak{g}$, and where $\langle\cdot,\cdot\rangle$ is the metric on $\mathfrak{g}$;

d *the curve $u(t)$ is an extremum of the reduced action function*

$$s(u) = \int l(u(t))dt,$$

for variations of the form

$$\delta u = \dot{w} + [w, u], \tag{A 4}$$

where $w = TR_{\eta^{-1}}\delta\eta$ vanishes at the endpoints.

See Chapter 13 in Marsden & Ratiu (1999) for a detailed development of the theory of Lagrangian reduction as well as a proof of the Euler-Poincaré theorem.

In the context of fluids, the right invariant Lagrangian $L : T\mathcal{D}_\mu(M) \to \mathbb{R}$ is simply the right invariant L^2 metric (A 2). The **reduced Lagrangian** $l : \mathcal{V}_\mu(M) \longrightarrow \mathbb{R}$ is the restriction of the L^2 metric to the Lie algebra given by (A 1); thus, the functional derivative $\delta l/\delta u$ computed with respect to (A 1) is equal to u. The **reduced action** s is defined on curves in $\mathcal{V}_\mu(M)$ and is given by

$$s(u) = \frac{1}{2}\int \langle u(t), u(t)\rangle_{L^2} dt. \tag{A 5}$$

One easily computes $\mathrm{ad}^*_u u$ in $\mathcal{V}_\mu(M)$ with respect to the L^2 metric (see Arnold & Khesin (1998), Chapter 1, Theorem 5.3) as

$$\mathrm{ad}^*_u u = \nabla_u u + \mathrm{grad}\ p,$$

so that critical points of s with respect to the constrained variations (A 4) are solutions of the Euler equations (A 3) by the Euler-Poincaré theorem.

REFERENCES

A. Arakawa, *Computational design for long-term numerical integration of the equations of fluid motion: Two-dimensional incompressible flow, Part 1*, J. Comput. Phys., **1**, (1966), 119-143.

V.I. Arnold and B. Khesin, *Topological Methods in Hydrodynamics*, Springer Verlag, New York, 1998.

V.I. Arnold, *Sur la geometrie differentielle des groupes de Lie de dimension infinie et ses applications a l'hydrodynamique des fluids parfaits*, Ann. Inst. Grenoble, **16**, (1966), 319–361.

G.I. Barenblatt and A.J. Chorin, *New Perspectives in turbulence: scaling laws, asymptotics, and intermittency*, SIAM Rev., **40**, (1998), 265–291.

G.I. Barenblatt and A.J. Chorin *Scaling laws and vanishing viscosity limits in turbulence theory*, Recent advances in partial differential equations, Venice 1996, Proc. Sympos. Appl. Math., **54**, 1–25.

C. Basdevant & R. Sadourny *Ergodic Properties of inviscid truncated models of two-dimensional incompressible flows*, J. Fluid Mech., **69**, (1975), 673–688.

C. Canuto, *Spectral methods in fluid dynamics*, Springer-Verlag, New York, 1988.

S. Chen, D.D. Holm, L. Margolin, and R. Zhang, *Direct numerical simulations of the Navier-Stokes alpha model*, (1999), preprint.

S. Chen, C. Foias, D.D. Holm, E. Olson, E. S. Titi, and S. Wynne, *The Camassa-Holm equations as a closure model for turbulent channel flow*, Phys. Rev. Lett., **81**, (1998), 5338–5341.

D. Cioranescu and E.H. Ouazar, *Existence and uniqueness for fluids of second grade*, In *Nonlinear Partial Differential Equations*, **109**, pp. 178–197. Collège de France Seminar, Pitman (1984).

D. Cioranescu and V. Girault, *Weak and classical solutions of a family of second grade fluids*, Inter. J. Non-Linear Mech., **32**, (1997), 317–335.

J.E. Dunn and R.L. Fosdick, *Thermodynamics, stability and boundedness of fluids of complexity* 2 *and fluids of second grade*, Arch. Rat. Mech. Anal., **56**, (1974), 191–252.

D. Ebin and J. Marsden, *Groups of diffeomorphisms and the motion of an incompressible fluid*, Ann. of Math., **92**, (1970), 102–163.

C. Foias, D.D. Holm and E.S. Titi, *Regularity of the Navier-Stokes-α equations*, in preparation.

D.G. Fox & S.A. Orszag, *Inviscid dynamics of two-dimensional turbulence*, Phys. Fluids, **16**, (1973), 169–171.

G.P. Galdi, M. Grobbelaarvandalsen, and N. Sauer, *Existence and uniqueness of classical-solutions of the equations of motion for 2nd-grade fluids*, Arch. Rat. Mech. Anal., **124**, (1993), 221–237.

D.D. Holm, J.E. Marsden, and T.S. Ratiu, *Euler-Poincaré equations and semidirect products with applications to continuum theories*, Adv. in Math., (1998), July 15.

D.D. Holm, J.E. Marsden, and T.S. Ratiu, *Euler-Poincaré models of ideal fluids with nonlinear dispersion*, Phys. Rev. Lett., **80**, (1998), 4273–4277.

R.H. Kraichnan, *Inertial ranges in two-dimensional turbulence*, Phys. Fluids, **10**, (1967), 1417–1423.

R.H. Kraichnan and D.Montgomery, *Two-dimensional turbulence*, Reports on progress in physics, **43**, (1980), 547–619.

A. Majda and M. Holen, Dissipation, topography, and statistical theories for large-scale coherent structure, Comm. Pure Appl. Math. **50**, (1997), 1183–1234.

J.E. Marsden and T.S. Ratiu, *Introduction to Mechanics and Symmetry*, Springer-Verlag, 2nd Edition, 1999.

J.E. Marsden, T.S. Ratiu, and S. Shkoller, *The geometry and analysis of the averaged Euler equations with normal boundary conditions*, Geom. Func. Anal., to appear

J.E. Marsden, T.S. Ratiu, and S. Shkoller, in preparation.

W.H. Matthaeus and D. Montgomery, *Selective decay hypothesis at high mechanical and magnetic reynolds-numbers*, Annals of the New York academy of sciences, **357**, (1980), 203–222.

J.C. McWilliams, *The emergence of isolated vortices in turbulent flow*, J. Fluid Mech., **146**, (1984), 21–34.

J. Miller, P.B. Weichman, and M.C. Cross, *Statistical-mechanics, Euler equation, and Jupiter's red spot*, Phys. Rev. A, **45**, (1992), 2328–2359.

B.T. Nadiga and L.G. Margolin, *Dispersive eddy parameterization in a barotropic ocean model*, in preparation.

B.T. Nadiga, and S. Shkoller, *Statistical scalings for the Euler-α equations*, in preparation.

W. Noll and C. Truesdell, *The nonlinear field theories of Mechanics*, Springer-Verlag, Berlin, (1965).

E.A. Overman and N.J. Zabusky, *Evolution and merging of isolated vortex structures*, Phys. Fluids, **25**, (1982), 1297–1305.

S. Pekarsky and S. Shkoller, *The curvature of $\mathcal{D}^s_\mu(\mathbb{T}^2)$ with H^1_α and stabilization of the Euler-α flow*, in preparation.

W.H. Press, B.P. Flannery, S.A.Teukolsky, & W.T. Vetterling, Numerical Recipes in Fortran 77, Cambridge University Press, (1992), 708–716.

R.S. Rivlin and J.L. Ericksen, *Stress-deformation relations for isotropic materials*, J. Rat. Mech. Anal. **4**, (1955), 323–425.

R. Robert and J. Sommeria, *Statistical equilibrium states for 2-dimensional flows*, J. Fluid Mech., **229**, (1991), 291–310.

S. Shkoller, *Geometry and curvature of diffeomorphism groups with H^1 metric and mean hydrodynamics*, J. Func. Anal., **160**, (1998), 337–365.

Appendix B. Figures

FIGURE B.1. Initial condition with minimum and maximum vorticity given by (-3.10,3.10).

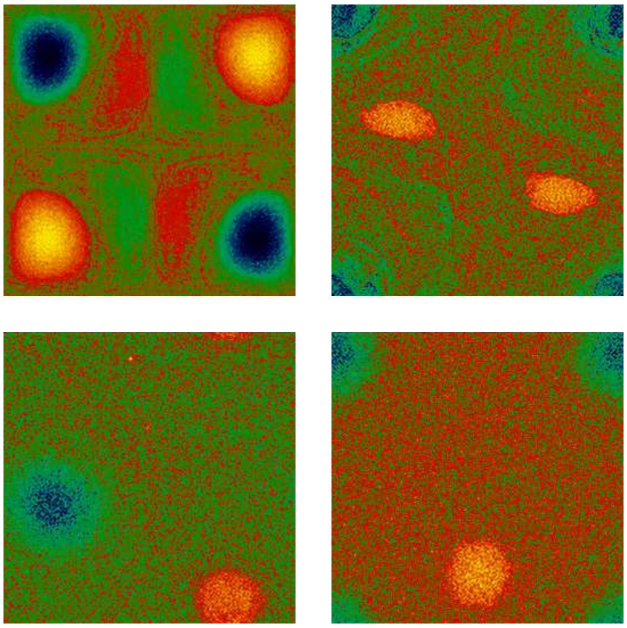

FIGURE B.2. Snapshots of the scaled vorticity field. (Truncated) Euler system. (a) Top Left: time 23 (large eddy turnover times); Mininum and maximum vorticity: $(-3.44,\ 3.45)$ (b) Top Right: time 46 $(-4.92,\ 5.07)$ (c) Bottom Left: time 69 $(-5.38,\ 6.05)$ (d) Bottom Right: time 92 $(-5.45,\ 4.89)$

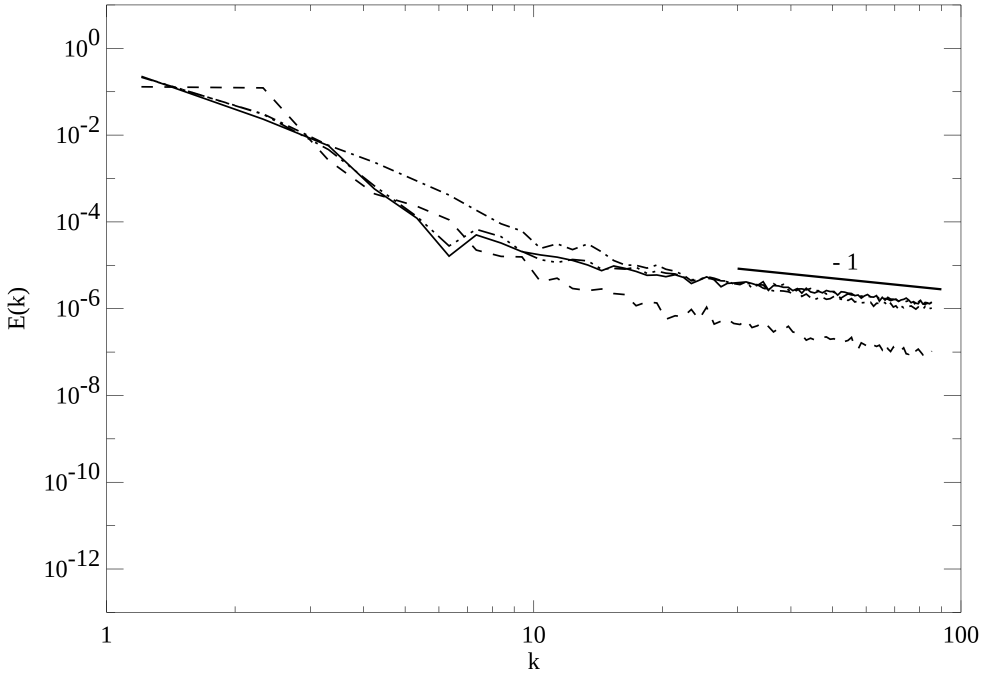

FIGURE B.3. Log-log plot of the instantaneous energy spectrum versus wave number at times 23, 46, 69 and 92

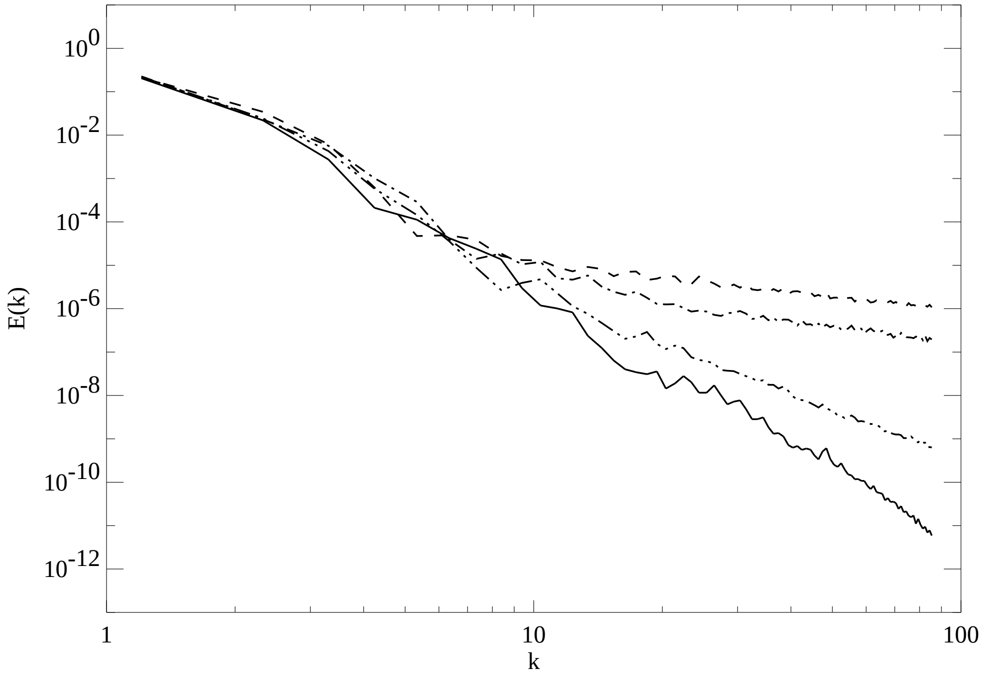

FIGURE B.4. The instantaneous energy spectrum at time 92 for the Navier-Stokes simulations with four different values of viscosity. Dashed line: 10^{-7}; Dot-dashed line: 10^{-6}; Dot-dot-dot-dashed line: 10^{-5}; Solid line: $5\,10^{-5}$. While the flow is not fully resolved in the first three cases, it is beginning to be marginally resolved in the case with the highest viscosity.

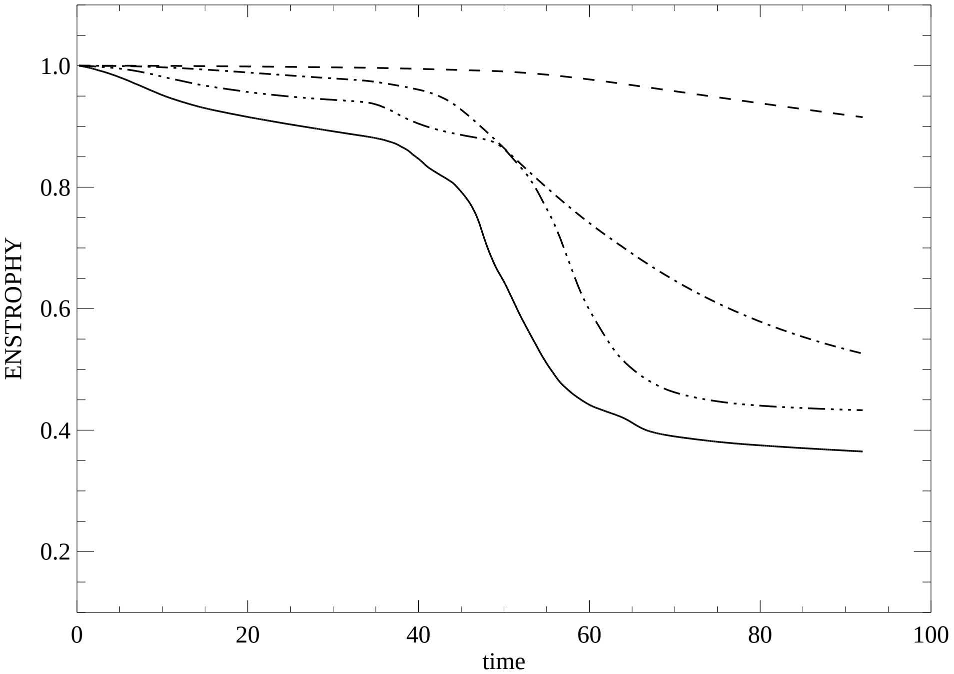

FIGURE B.5. Evolution of enstrophy with time for the Navier-Stokes simulations with four different values of viscosity. Dashed line: 10^{-7}; Dot-dashed line: 10^{-6}; Dot-dot-dot-dashed line: 10^{-5}; Solid line: $5\,10^{-5}$. Normalization is by the enstrophy conserved in the Euler simulation.

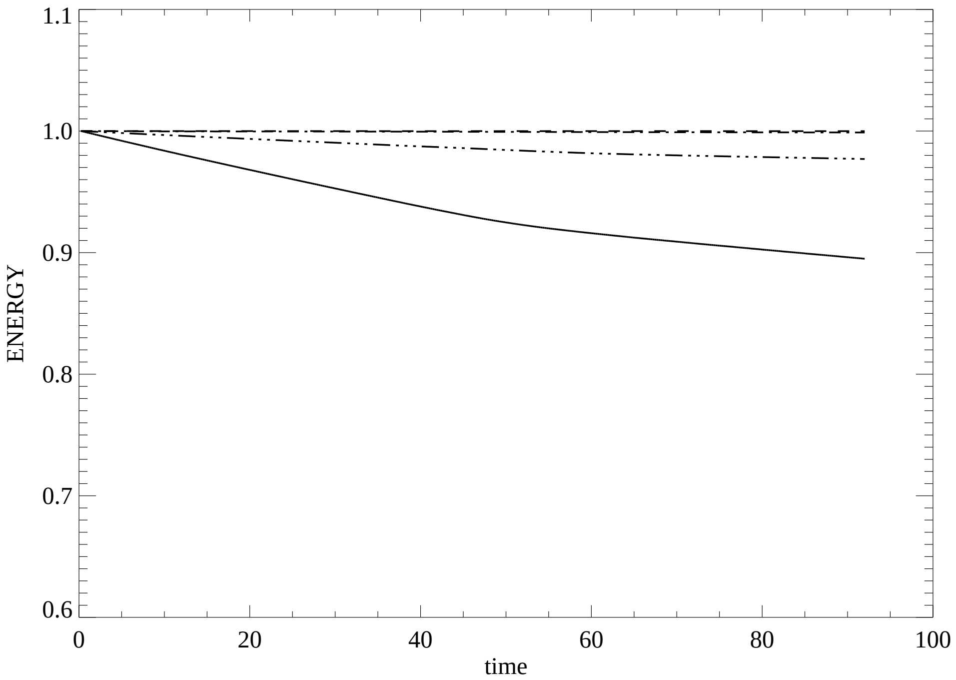

FIGURE B.6. Evolution of energy with time for the Navier-Stokes simulations with four different values of viscosity. Dashed line: 10^{-7}; Dot-dashed line: 10^{-6}; Dot-dot-dot-dashed line: 10^{-5}; Solid line: $5\,10^{-5}$. Normalization is by the energy conserved in the Euler simulation.

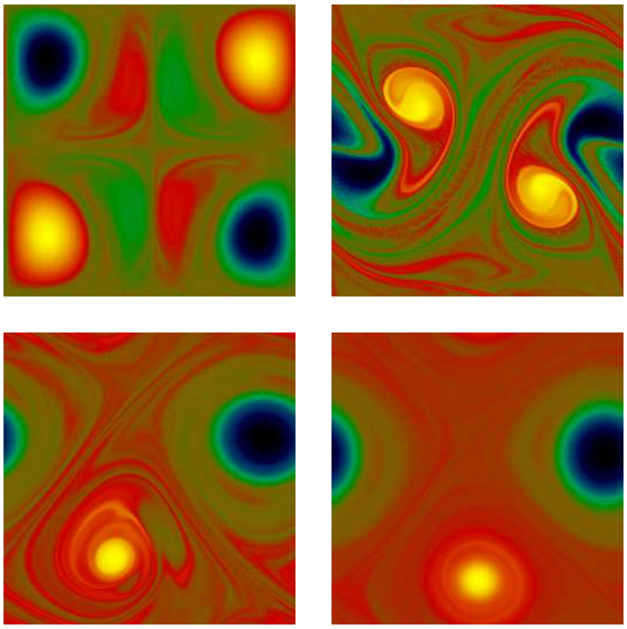

FIGURE B.7. Snapshots of the scaled vorticity field. Navier-Stokes equations with a viscosity of $5\,10^{-5}$. (a) Top Left: time 23 (large eddy turnover times); Mininum and maximum vorticity: $(-3.02,\ 3.02)$ (b) Top Right: time 46 $(-3.04,\ 2.98)$ (c) Bottom Left: time 69 $(-2.77,\ 2.64)$ (d) Bottom Right: time 92 $(-2.72,\ 2.55)$

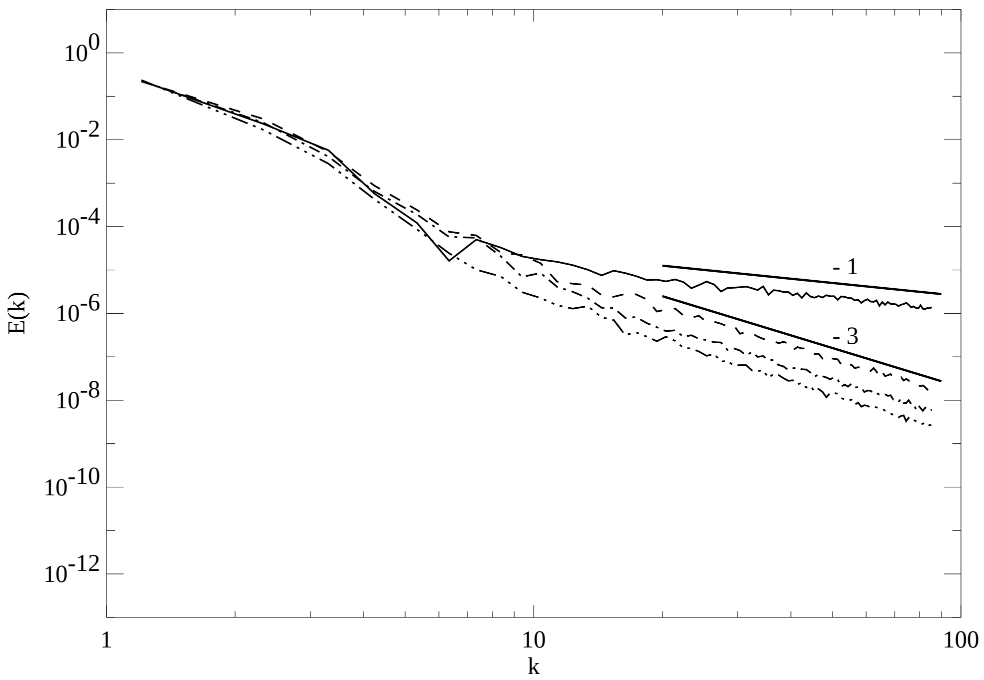

FIGURE B.8. Instantaneous spectra at time 92 for the truncated Euler system (Solid line) and the truncated Euler-α system with three different values of α. Dashed line: 0.1; Dot-dashed line: 0.2; Dot-dot-dot-dashed line: 0.4. Slopes of k^{-1} and k^{-3} are shown for reference.

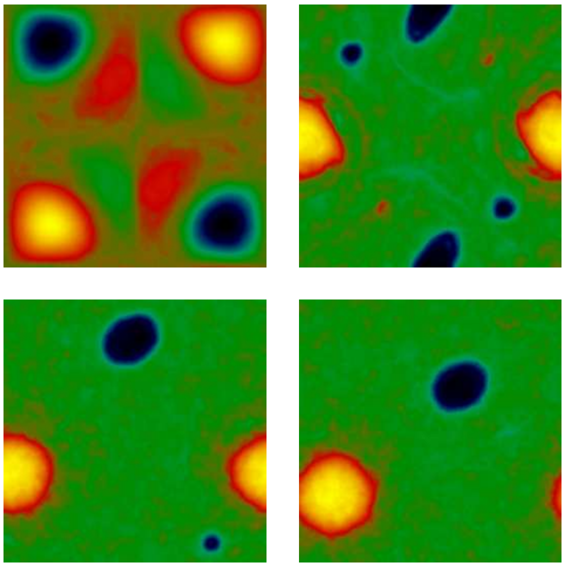

FIGURE B.9. Snapshots of the scaled vorticity field ω^α. Euler-α equations with α=0.1. (a) Top Left: time 23 (large eddy turnover times); Mininum and maximum vorticity: $(-3.02, 3.02)$ (b) Top Right: time 46 $(-2.41, 2.97)$ (c) Bottom Left: time 69 $(-2.51, 3.01)$ (d) Bottom Right: time 92 $(-2.50, 3.00)$

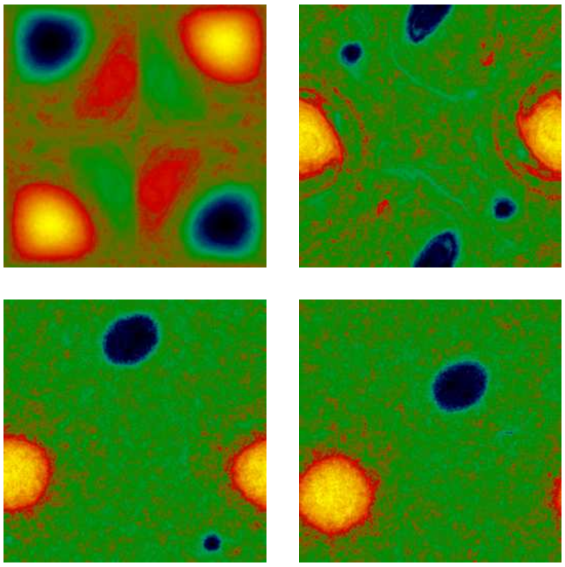

FIGURE B.10. Snapshots of the roughened vorticity field, for the same α-run. (a) Top Left: time 23 (large eddy turnover times); Mininum and maximum vorticity: $(-3.13, 3.13)$ (b) Top Right: time 46 $(-2.80, 3.22)$ (c) Bottom Left: time 69 $(-2.74, 3.25)$ (d) Bottom Right: time 92 $(-2.81, 3.26)$

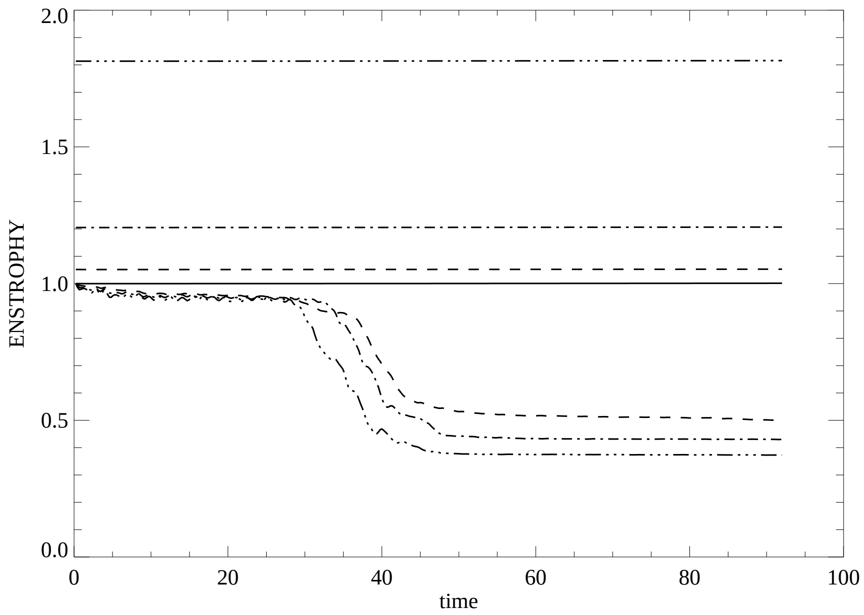

FIGURE B.11. Evolution of enstrophies—$Z(F_\alpha^2\omega^\alpha)$ (which are conserved and $Z(F_\alpha\omega^\alpha)$—for the Euler-α simulations with four different values of α. Solid line: $\alpha = 0$; Dashed line: $\alpha = 0.1$; Dot-dashed line: $\alpha = 0.2$; Dot-dot-dot-Dashed line: $\alpha = 0.4$. Normalization is by the enstrophy conserved by the Euler simulation.

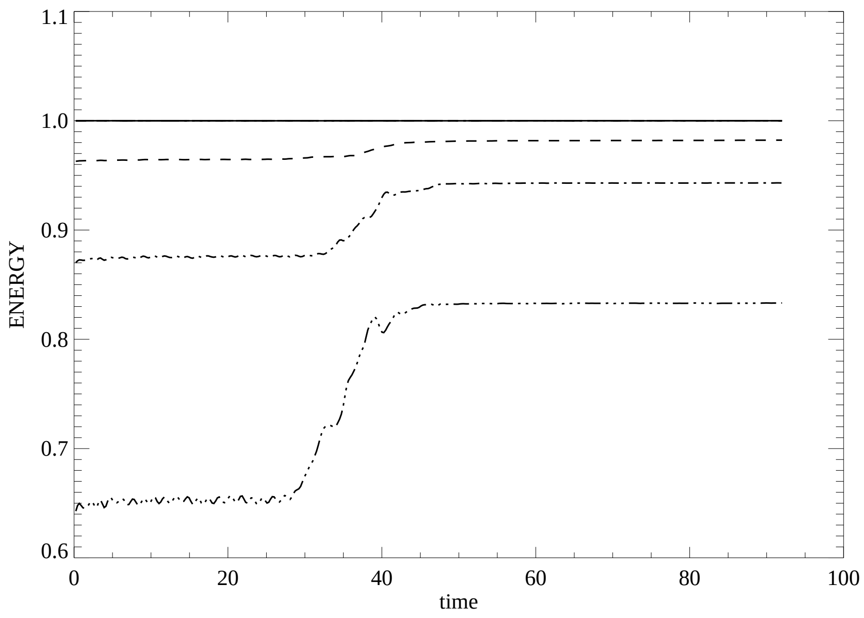

FIGURE B.12. Evolution of energies—$K(F_\alpha\psi^\alpha)$ (which are conserved) and $K(\psi^\alpha)$—for the Euler-α simulations with four different values of α. Solid line: $\alpha = 0$; Dashed line: $\alpha = 0.1$; Dot-dashed line: $\alpha = 0.2$; Dot-dot-dot-Dashed line: $\alpha = 0.4$. Normalization is by the energy conserved by the Euler simulation.

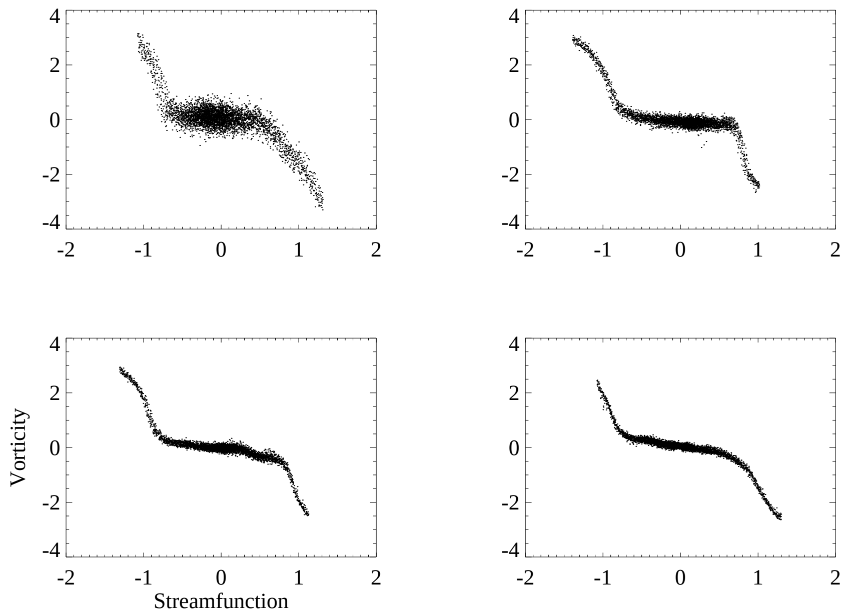

FIGURE B.13. Scatter plots of instantaneous vorticity, $F_\alpha \omega^\alpha$, and streamfunction, ψ^α at time 92 for the truncated Euler and Euler-α systems. Top Left: $\alpha = 0$ (Euler); Top Right: $\alpha = 0.1$; Bottom Left: $\alpha = 0.2$; Bottom Right: $\alpha = 0.4$.